Numerical simulations of an effective model of QCD with two light quark flavors

José Antonio García Hernández
Edgar López Contreras
Wolfgang Bietenholz

Instituto de Ciencias Nucleares
Universidad Nacional Autónoma de México

MexNICA December 2020

Outline

Lattice QCD

- Lattice QCD is a succesful non-perturbative approach, but

$$\mu_B > 0 \Rightarrow S_{\text{QCD,E}},\ e^{-S_{\text{QCD, E}}} \in \mathbb{C}\,.$$

- Reweighting: Absorb the imaginary part into the observable and generate configurations with the real part.
- The sign problem
$\langle O \rangle$ mostly cancellations $\Rightarrow$ requires huge statistics $\propto e^{cV}$.
- The *sign problem* has prevented numerical simulations at finite baryon density.

QCD Phase Transition as Chiral Symmetry Breaking

Considering massless quark flavors

$$\mathcal{L}_{\mathrm{E,QCD}} = \sum_{\mathrm{f}} \left(\bar{\psi}_{\mathrm{L,f}} \not{D} \psi_{\mathrm{L,f}} + \bar{\psi}_{\mathrm{R,f}} \not{D} \psi_{\mathrm{R,f}} \right) + \frac{1}{4} \mathrm{Tr}[G_{\mu\nu} G_{\mu\nu}] \,,$$

is invariant under
$U(2)_L \otimes U(2)_R = SU(2)_L \otimes SU(2)_R \otimes U(1)_{L=R} \otimes U(1)_{L\neq R}$
transformations

$$\psi_{L,R} = \frac{1}{2}(1 \pm \gamma_5)\psi,\ \bar{\psi}_{L,R} = \bar{\psi}\frac{1}{2}(1 \mp \gamma_5).$$

The Chiral Symmetry breaks spontaneously

$$SU(2)_L \otimes SU(2)_R \simeq O(4) \to SU(2)_{L=R} \simeq O(3)\,,$$

which gives rise to 3 Nambu-Goldstone bosons (NGBs).

Effective 2-flavor QCD Lagrangian

$$\mathcal{L}_{eff} = \frac{F_\pi^2}{4} \mathrm{Tr}[\partial_\mu U^\dagger \partial_\mu U]\,,$$

where $U \in SU(2)_L \otimes SU(2)_R / SU(2)_{L=R} = SU(2)$, and $F_\pi = 92.4$ MeV.

Equivalently, with fields $\vec{e}(x) \in S^3$

$$\mathcal{L}_{eff} = \frac{F_\pi^2}{2} \partial_\mu \vec{e}(x) \cdot \partial_\mu \vec{e}(x)\,,$$

The 2-flavor QCD Lagrangian is a non-linear σ-model or O(4) model.

The inclusion of quark masses

Since quarks have masses, chiral symmetry is approximate.

Mass term

$$\sum_{\mathrm{f}} m_{\mathrm{f}} \left(\bar{\Psi}_{\mathrm{fL}}(x)\Psi_{\mathrm{fR}}(x) + \bar{\Psi}_{\mathrm{fR}}(x)\Psi_{\mathrm{fL}}(x) \right)$$

For degenerate quark masses m, we have a symmetry under simultaneous transformations in $SU(2)_{L=R}$.

In our effective theory, a *magnetic field* $\vec{h}$ breaks explicitly the O(4) down to O(3)

$$\mathcal{L}_{\mathrm{eff}} = \frac{F_\pi^2}{2} \partial_\mu \vec{e}(x) \cdot \partial_\mu \vec{e}(x) - \vec{h} \cdot \vec{e}(x)$$

where $\vec{e}(x) \in S^3$.

Dimensional reduction

We assume a 4-d volume of the form $\beta \times V$, where $\beta = 1/T$ is the extent of Euclidean time, and $V = L^3$.

The Euclidean action reads

$$S_{\mathrm{E}}[\vec{e}] = \int_0^{\beta} dt_{\mathrm{E}} \int_V d^3x \left(\frac{F_\pi^2}{2} \partial_\mu \vec{e}(x) \cdot \partial_\mu \vec{e}(x) - \vec{h} \cdot \vec{e}(x) \right) .$$

We consider the case of high temperature $T = 1/\beta$

$$S_{\mathrm{E}}[\vec{e}] = \beta \underbrace{\int_V d^3x \left(\frac{F_\pi^2}{2} \partial_i \vec{e}(x) \cdot \partial_i \vec{e}(x) - \vec{h} \cdot \vec{e}(x) \right)}_{H[\vec{e}]} ,$$

this simplification is known as *dimensional reduction*.

The inclusion of μ_B

The topological charge takes the role of the baryon number (Skyrme (1961)). In our effective theory

$$H[\vec{e}] = \int_V d^3x \left(\frac{F_\pi^2}{2} \partial_\mu \vec{e}(x) \cdot \partial_\mu \vec{e}(x) - \vec{h} \cdot \vec{e}(x) \right) - \mu_B Q[\vec{e}] \,.$$

Lattice regularization

We regularize the path integral by means of the lattice regularization, with lattice spacing $a = 1$.

The lattice Hamiltonian is written as

$$H_{\mathrm{lat}}[\vec{e}] = -F_\pi^2 a \sum_x \sum_i \vec{e}_{x+a\hat{\imath}} \cdot \vec{e}_x - \mu_B Q[\vec{e}] - a^3 \vec{h} \cdot \sum_x \vec{e}_x \,.$$

$$S_{\mathrm{E,lat}}[\vec{e}] = \beta_{\mathrm{lat}} H_{\mathrm{lat}}[\vec{e}]$$

Considering massless quarks, simulations show $\beta_{c,\mathrm{lat}} = 0.93590$ Oevers (1996); Engels et al. (2003).

Identifying this value with the crossover temperature $T_x = 155$ MeV Bhattacharya et al. (2014), we used the ratio $\beta_x/\beta_{c,\mathrm{lat}}$ to convert $\mu_{B,\mathrm{lat}}$ and h_{lat} into physical units.

We need to estimate h_{lat} realistically

$$h_{\mathrm{lat}} = h\frac{\beta_x^4}{\beta_{c,\mathrm{lat}}^4} = h(145.1\,\mathrm{MeV})^{-4}\,.$$

According to the Gell-Mann–Oakes–Renner relation

$$h = m_q \Sigma = F_\pi^2 M_\pi^2 \approx (92.4\,\mathrm{MeV})^2 (138\,\mathrm{MeV})^2$$
$$= (112.9\,\mathrm{MeV})^4 = 1.626 \times 10^8\,\mathrm{MeV}^4 \,.$$

Therefore

$$h_{\mathrm{lat}} \approx 0.367.$$

This value corresponds to a quark mass of

$$m_q = \frac{F_\pi^2 M_\pi^2}{\Sigma} = \frac{1.626 \times 10^8\,\mathrm{MeV}^4}{(250\,\mathrm{MeV})^3} \approx 10.4\,\mathrm{MeV}\,.$$

What matters is that we account for the correct pion mass.

Monte Carlo Methods

Local update algorithms have problems, they suffer from **critical slowing down**.

Critical slowing down means that near a critical point it becomes exponentially hard for the simulation to generate statistically independent configurations.

Cluster algorithms, such as the **Wolff algorithm**, suppress critical slowing down.

We use the 3-d O(4) model as an effective theory.

We monitor the temperature $T = 1/\beta$ where the crossover takes place, to explore the QCD phase diagram with two massive quark flavors at finite baryon density.

This is done numerically using the Wolff algorithm that supressess critical slowing down.

Simulation parameters

- We simulated the lattice 3-d O(4) model with cubic volumes $V = L^3$ with periodic boundary conditions at $h_{\mathrm{lat}} = 0.367$, $\mu_{\mathrm{lat},B} = \{0, 0.2, \ldots, 2\}$ and several temperatures.
- We took 5×10^4 measurements, separated by 10 multi-cluster updates.
- We measured observables such as the energy density, magnetization, topological charge, specific heat, magnetic susceptibility, etc.

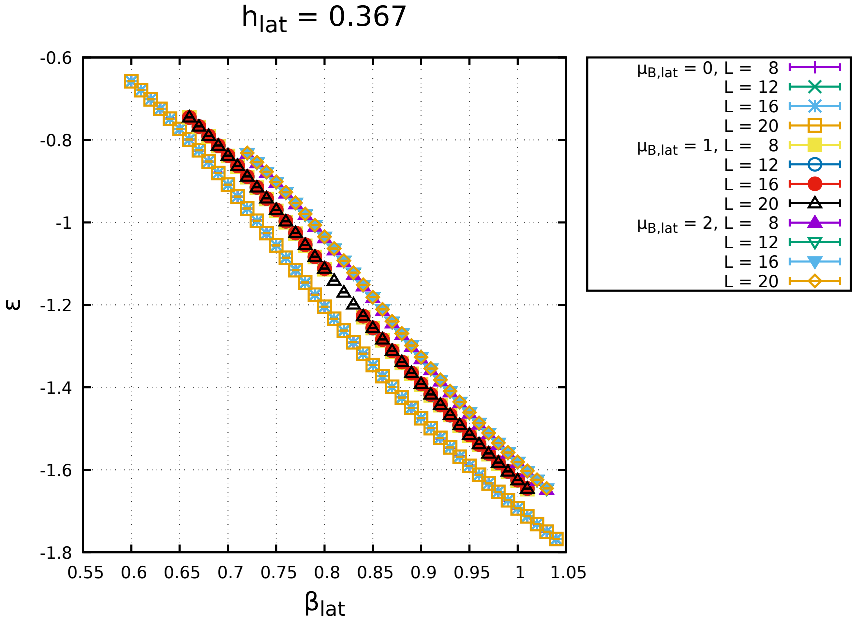

h_lat = 0.367
-0.6
-0.8
-1
-1.2
-1.4
-1.6
-1.8
ω
0.55 0.6 0.65 0.7 0.75 0.8 0.85 0.9 0.95 1 1.05
β_lat
μ_B,lat = 0, L = 8
L = 12
L = 16
L = 20
μ_B,lat = 1, L = 8
L = 12
L = 16
L = 20
μ_B,lat = 2, L = 8
L = 12
L = 16
L = 20

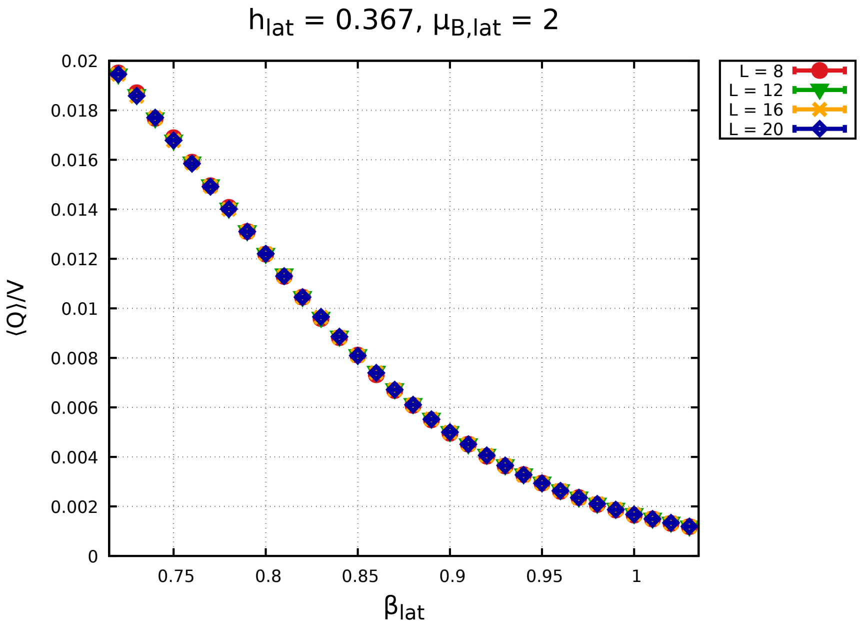

$h_{lat} = 0.367, \mu_{B,lat} = 2$
⟨Q⟩/V
0.02
0.018
0.016
0.014
0.012
0.01
0.008
0.006
0.004
0.002
0
0.75
0.8
0.85
0.9
0.95
1
β_{lat}
L = 8
L = 12
L = 16
L = 20

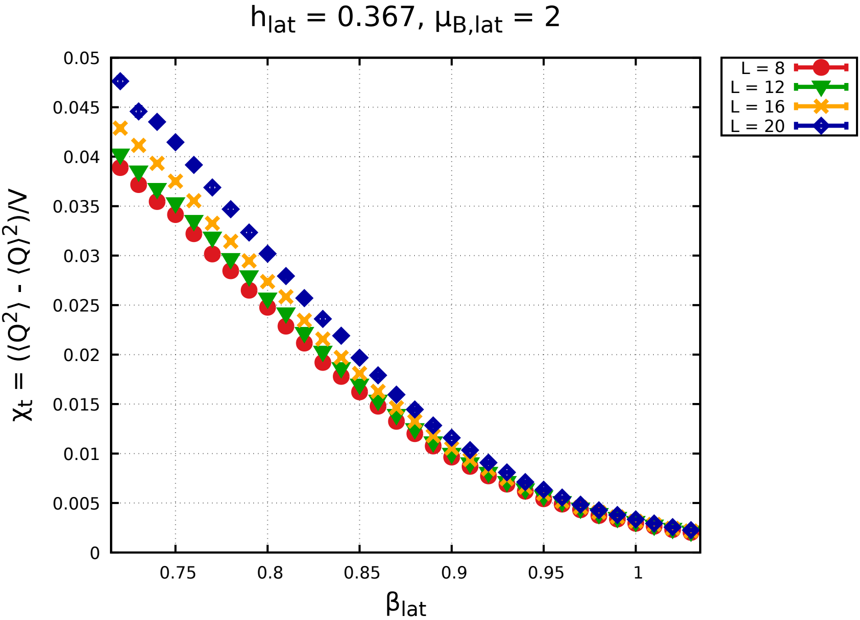

$h_{lat} = 0.367,\ \mu_{B,lat} = 2$
$\chi_t = (\langle Q^2 \rangle - \langle Q \rangle^2)/V$
β_{lat}
L = 8
L = 12
L = 16
L = 20
0.05
0.045
0.04
0.035
0.03
0.025
0.02
0.015
0.01
0.005
0
0.75
0.8
0.85
0.9
0.95
1

$h_{lat} = 0.367$, $L = 20$

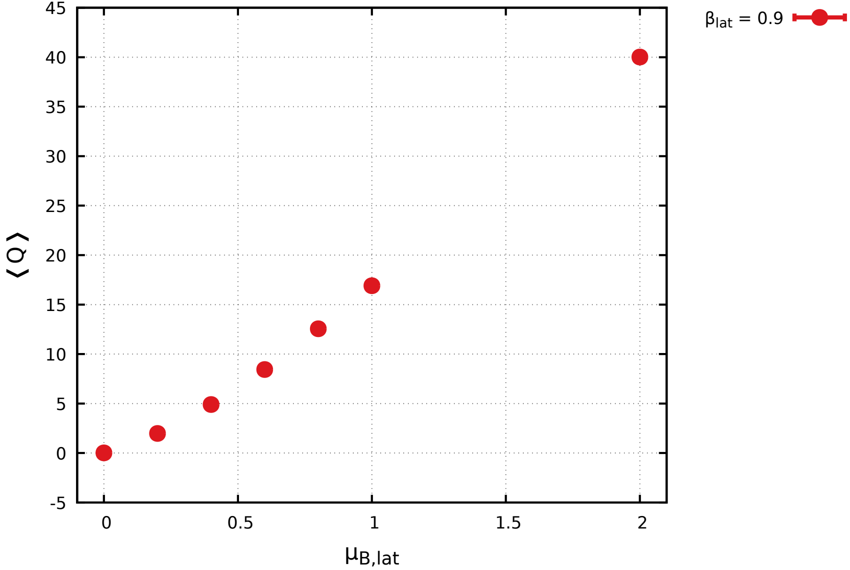

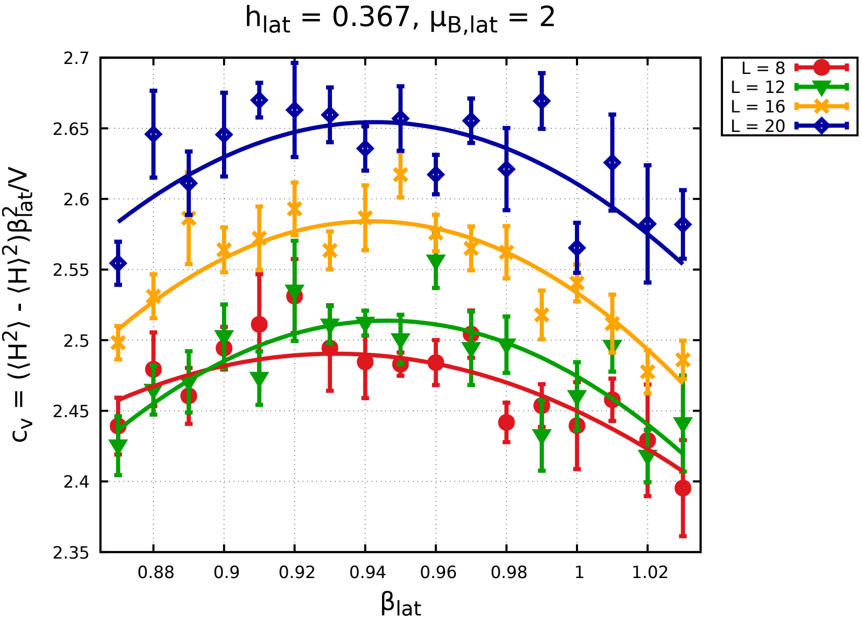

$h_{lat} = 0.367$, $\mu_{B,lat} = 2$
L = 8
L = 12
L = 16
L = 20
2.7
2.65
2.6
2.55
2.5
2.45
2.4
2.35
0.88
0.9
0.92
0.94
0.96
0.98
1
1.02
$c_V = (\langle H^2 \rangle - \langle H \rangle^2)\beta_{lat}^2/V$
β_{lat}

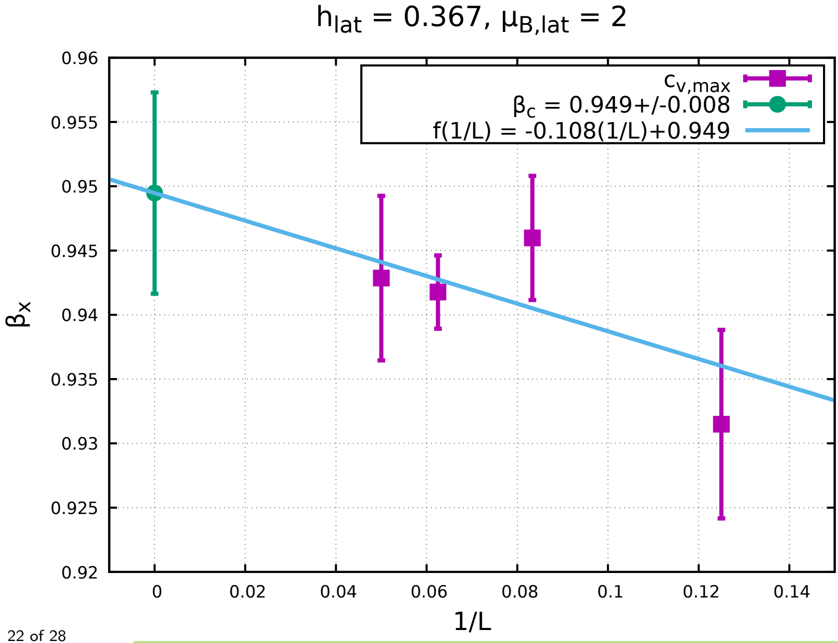
$h_{lat} = 0.367$, $\mu_{B,lat} = 2$
$c_{v,max}$
$\beta_c = 0.949 +/- 0.008$
$f(1/L) = -0.108(1/L)+0.949$
0.96
0.955
0.95
0.945
0.94
0.935
0.93
0.925
0.92
β_X
0
0.02
0.04
0.06
0.08
0.1
0.12
0.14
1/L

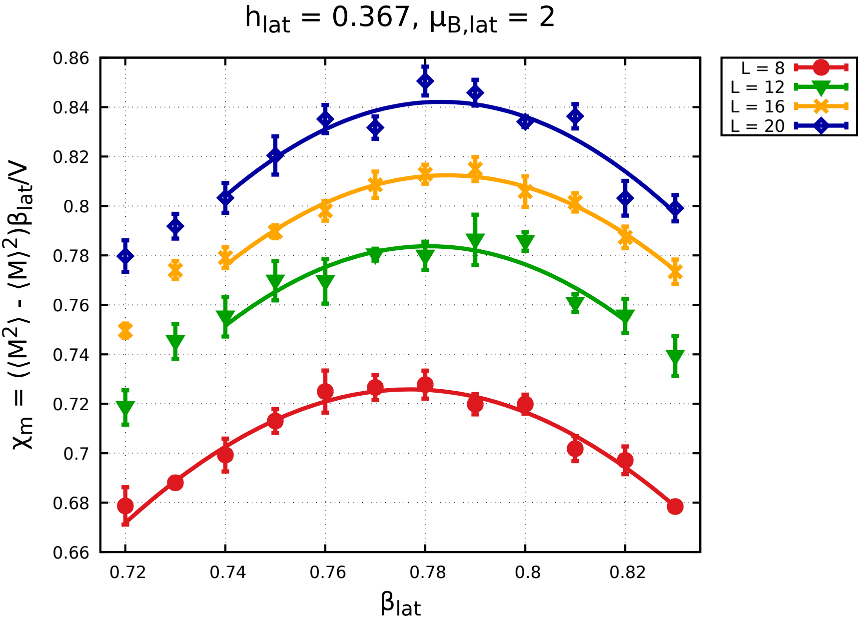

h_{lat} = 0.367, $\mu_{B,lat}$ = 2
L = 8
L = 12
L = 16
L = 20
$\chi_m = (\langle M^2\rangle - \langle M\rangle^2)\beta_{lat}/V$
β_{lat}
0.66
0.68
0.7
0.72
0.74
0.76
0.78
0.8
0.82
0.84
0.86
0.72
0.74
0.76
0.78
0.8
0.82

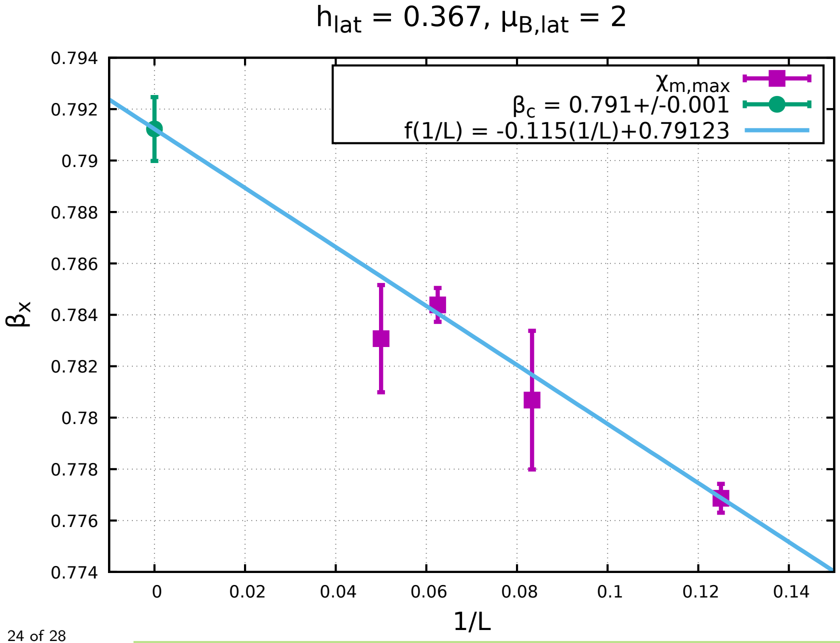
$h_{lat} = 0.367,\ \mu_{B,lat} = 2$
$\chi_{m,max}$
β_c = 0.791+/-0.001
f(1/L) = -0.115(1/L)+0.79123
β_x
1/L
0.794
0.792
0.79
0.788
0.786
0.784
0.782
0.78
0.778
0.776
0.774
0
0.02
0.04
0.06
0.08
0.1
0.12
0.14

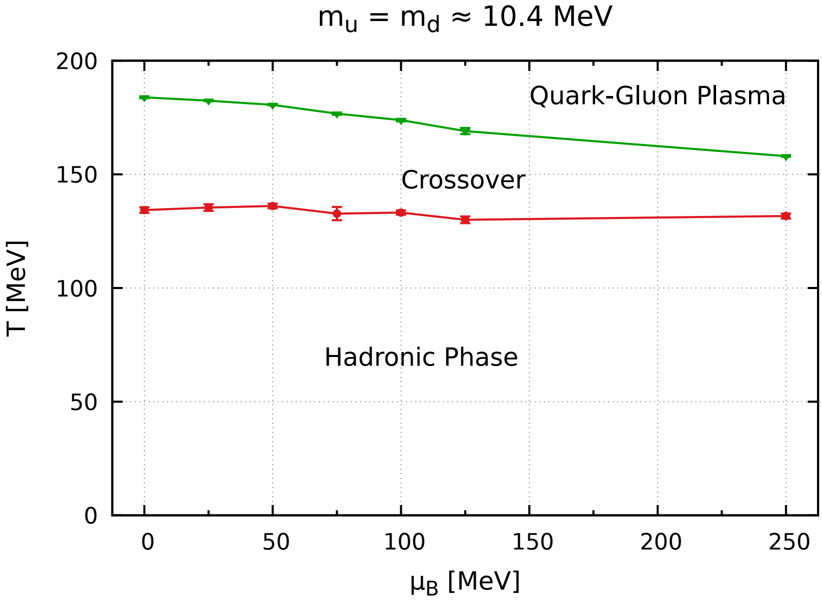
$m_u = m_d \approx 10.4$ MeV
200
150
100
50
0
T [MeV]
Quark-Gluon Plasma
Crossover
Hadronic Phase
0
50
100
150
200
250
μ_B [MeV]

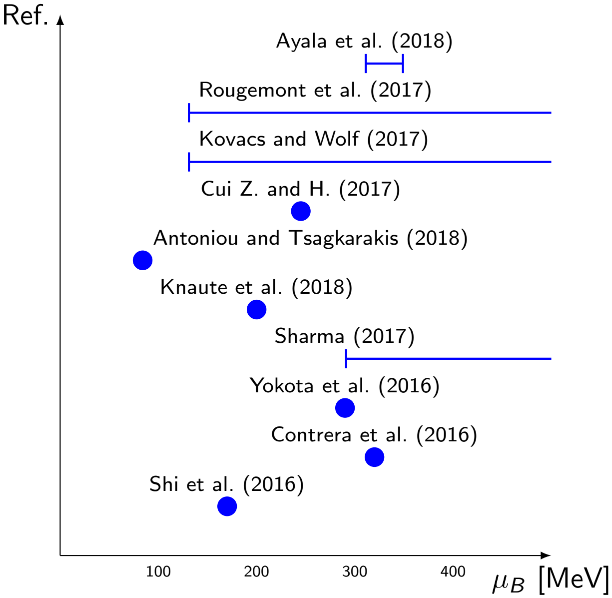
Ref.
Ayala et al. (2018)
Rougemont et al. (2017)
Kovacs and Wolf (2017)
Cui Z. and H. (2017)
Antoniou and Tsagkarakis (2018)
Knaute et al. (2018)
Sharma (2017)
Yokota et al. (2016)
Contrera et al. (2016)
Shi et al. (2016)
100
200
300
400
μ_B [MeV]

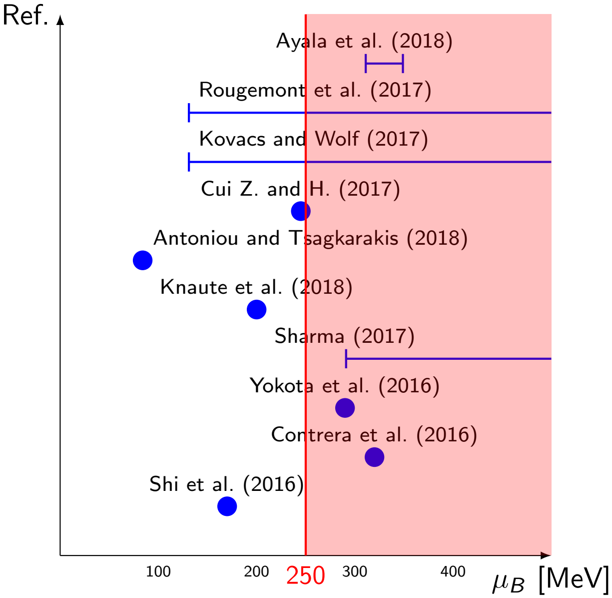

Ref.
Ayala et al. (2018)
Rougemont et al. (2017)
Kovacs and Wolf (2017)
Cui Z. and H. (2017)
Antoniou and Tsagkarakis (2018)
Knaute et al. (2018)
Sharma (2017)
Yokota et al. (2016)
Contrera et al. (2016)
Shi et al. (2016)
100
200
250
300
400
μ_B [MeV]

Conclusions

- We used the 3-d O(4) model as an effective theory to study the QCD phase diagram.
- An external magnetic field accounts for a denegenerate quark mass.
- We plotted the phase diagram to energies up to 250 MeV of the chemical potential μ_B.
- A CEP was not observed in this range μ_B.

Conclusions

- We used the 3-d O(4) model as an effective theory to study the QCD phase diagram.
- An external magnetic field accounts for a denegenerate quark mass.
- We plotted the phase diagram to energies up to 250 MeV of the chemical potential μ_B.
- A CEP was not observed in this range μ_B.

Conclusions

- We used the 3-d O(4) model as an effective theory to study the QCD phase diagram.
- An external magnetic field accounts for a denegenerate quark mass.
- We plotted the phase diagram to energies up to 250 MeV of the chemical potential μ_B.
- A CEP was not observed in this range μ_B.

Conclusions

- We used the 3-d O(4) model as an effective theory to study the QCD phase diagram.
- An external magnetic field accounts for a denegenerate quark mass.
- We plotted the phase diagram to energies up to 250 MeV of the chemical potential μ_B.
- A CEP was not observed in this range μ_B.

Outlook

- Increase volumes.
- Explore higher μ_B.

Outlook

- Increase volumes.
- Explore higher μ_B.

Antoniou, N. Diakonos, F. M. X. and Tsagkarakis, C. (2018). Locating the QCD critical endpoint through finite-size scaling. *Phys. Rev. D*, 97.

Ayala, A., Hernández-Ortiz, S., and Hernández, L. (2018). QCD phase diagram from chiral symmetry restoration: analytic approach at high and low temperature using the linear sigma model with quarks. *Rev. Mex. Fis.*, 64:302–313.

Bhattacharya, T., Buchoff, M. I., Christ, N. H., Ding, H.-T., Gupta, R., Jung, C., Karsch, F., Lin, Z., Mawhinney, R. D., McGlynn, G., Mukherjee, S., Murphy, D., Petreczky, P., Renfrew, D., Schroeder, C., Soltz, R. A., Vranas, P. M., and Yin, H. (2014). QCD Phase Transition with Chiral Quarks and Physical Quark Masses. *Phys. Rev. Lett.*, 113:082001.

Contrera, G. A., Grunfeld, A. G., and Blaschke, D. (2016). Supporting the search for the CEP location with nonlocal PNJL models constrained by lattice QCD. 52:231.

Cui Z., Z. J. and H., Z. (2017). Proper time regularization and the QCD chiral phase transition. *Sci. Rep.*, 7:45937.

Engels, J., Fromme, L., and Seniuch, M. (2003). Correlation lengths and scaling functions in the three-dimensional O(4) model. *Nuc. Phys. B*, 675:533–554.

Knaute, J., Yaresko, R., and Kämpfer, B. (2018). Holographic QCD phase diagram with critical point from Einstein–Maxwell-dilaton dynamics. *Physics Letters B*, 778:419 – 425.

Kovacs, P. and Wolf, G. (2017). Phase diagram and isentropic curves from the vector meson extended Polyakov quark meson model.

Oevers, M. (1996). *The finite temperature phase diagram of 2-flavour QCD with improved Wilson fermions*. PhD thesis, Universität Biefeld.

Rougemont, R., Critelli, R., Noronha-Hostler, J., Noronha, J., and Ratti, C. (2017). Dynamical versus equilibrium properties of the QCD phase transition: A holographic perspective. *Phys. Rev. D*, 96:014032.

Sharma, S. (2017). The QCD Equation of state and critical end-point estimates at O(μB6). *Nuc. Phys. A*, 967:728 – 731.

Shi, C., Du, Y.-L., Xu, S.-S., Liu, X.-J., and Zong, H.-S. (2016). Continuum study of the QCD phase diagram through an OPE-modified gluon propagator. *Phys. Rev. D*, 93:036006.

Skyrme, T. H. R. (1961). A nonlinear field theory. *Proc. Roy. Soc. Lond.*, A260:127–138.

Yokota, T., Kunihiro, T., and Morita, K. (2016). Spectral functions in functional renormalization group approach – analysis of the collective soft modes at the QCD critical point –.